JOURNAL OF GEOPHYSICAL RESEARCH, VOL. 98, NO. C4, PAGES 7011–7022, APRIL 15, 1993

A Modified Galerkin-Spectral Model for Three-Dimensional, Barotropic, Wind-Driven Shelf Circulation

JINYU SHENG AND KEITH R. THOMPSON

Department of Oceanography, Dalhousie University, Halifax, Nova Scotia, Canada

We describe an efficient numerical scheme for calculating wind-driven currents on the continental shelf. Our scheme is based on the spectral approach introduced by Heaps and subsequently modified by Lardner. The basic idea behind Heaps' approach is to express the horizontal flow, $\mathbf{u}(x, y, z, t)$, as a linear combination of vertical structure functions, $\phi_r(z)$, and then solve numerically for the temporally and horizontally varying coefficients. To obtain an accurate representation of wind-driven flow, many ϕ_r are often required. Following Lardner, we reduce this number by subtracting from $\mathbf{u}$ an analytically defined flow field, $\mathbf{u}_P$, prior to its expansion in terms of the ϕ_r. Our choice of $\mathbf{u}_P$ is steady Ekman flow in water of finite depth. This particular choice includes, as a special case, the $\mathbf{u}_P$ used by Lardner. Using an idealized basin and time-harmonic wind forcing, we compare the convergence rate of the expansion of $\mathbf{u} - \mathbf{u}_P$ with $\mathbf{u}_P$ taken to be (1) zero, corresponding to Heaps' approach, (2) flow with constant horizontal shear stress through the vertical, corresponding to Lardner's recent suggestion, and (3) steady Ekman flow. We find that removal of steady Ekman flow generally leads to the most rapid convergence, particularly when the water depth is much greater than the Ekman depth, a condition often found on the middle and outer continental shelf.

1. INTRODUCTION

Over the last 2 decades the spectral method has been used with considerable success to compute three-dimensional, wind-driven currents and tidal streams over the continental shelf during the periods of weak stratification. The underlying idea is to express the horizontal flow, $\mathbf{u}(x, y, z, t)$, as a linear combination of vertical structure functions, $\phi_r(z)$, with coefficients that vary with x, y, and t. The ϕ_r are normally taken to be orthogonal, and so by vertically integrating the product of the momentum equation with each ϕ_r, a set of equations governing the evolution of their coefficients can be readily obtained. *Heaps* [1972] was one of the first physical oceanographers to apply this approach in his seminal study of wind-driven motion in a rectangular shelf sea of constant water depth and constant eddy viscosity. Later, Davies [e.g., *Davies*, 1980, 1983, 1988] and others [e.g., *Furnes*, 1983; *Lardner*, 1990] extended Heaps' approach to accommodate arbitrary eddy viscosity profiles, using a variety of vertical structure functions that include cosines, Chebyshev polynomials, B splines, and piecewise linear functions. To improve the computational efficiency of Heaps' approach, a time-splitting technique has also been introduced [*Davies*, 1987] whereby the first mode is integrated with a time step limited by the CFL condition, while the other modes integrated with a longer time step. The present generation of spectral models have been developed to the point that they are now extremely useful tools for studying the three-dimensional circulation over the continental shelf. (See *Davies* [1987] for a comprehensive review.)

It has been known for some time, however, that if the ϕ_r are taken to be the eigenfunctions associated with the eddy viscosity profile, convergence can be slow for the wind-driven component of the flow, particularly in the high-shear zone close to the sea surface. The result is that many ϕ_r may be required to accurately describe surface currents [e.g., *Davies*, 1987]. In an attempt to accelerate the convergence, *Davies and Owen* [1979] showed that accurate solutions could be obtained using relatively few Chebyshev polynomials because these functions are highly sheared close the surface and bottom. It was also found, however, that Chebyshev polynomials have a high computational overhead and the rapid rate of convergence is offset by their computational cost [*Davies and Stephens*, 1983]. Recently, *Lardner* [1990], *Davies* [1991, 1992], and *Zitman* [1992] have demonstrated that with minimal additional computational cost, convergence can be accelerated by first subtracting from $\mathbf{u}$ a particular flow field, $\mathbf{u}_P$, leaving a "remainder," $\mathbf{u}_R$, that can be accurately represented with far fewer vertical structure functions ϕ_r than would be possible otherwise. Lardner's choice for $\mathbf{u}_P$ was flow with constant horizontal shear stress through the vertical. *Davies* [1991, 1992] has suggested that $\mathbf{u}_P$ be decomposed into two parts: one proportional to the surface wind stress and the other proportional to the bottom shear stress. Each component is a quadratic function in the vertical and nonzero only in the region close to the boundary layer. Zitman's choice of $\mathbf{u}_P$ is proportional to the product of the surface wind stress and one of the eigenfunctions of the eddy viscosity profile, with nonzero gradient at the sea surface.

As part of an interdisciplinary study of cod recruitment in the northwest Atlantic, a group of biological and physical oceanographers in the Ocean Production Enhancement Network are attempting to track a cohort of cod larvae on the Scotian shelf in order to determine those factors controlling survival during the cod's early life history. The main contribution of the physical oceanographers will be to provide nowcasts and short-term forecasts of the circulation so that the biologists can focus their sampling effort on the same group of individuals and thus determine what is special about the larvae that survive. We are tackling this physical oceanographic problem using a limited-area circulation model which is driven with observed winds and flows across the open boundary. These boundary flows cannot be observed in

Paper number 92JC02963.
0148-0227/93/92JC-02963$05.00

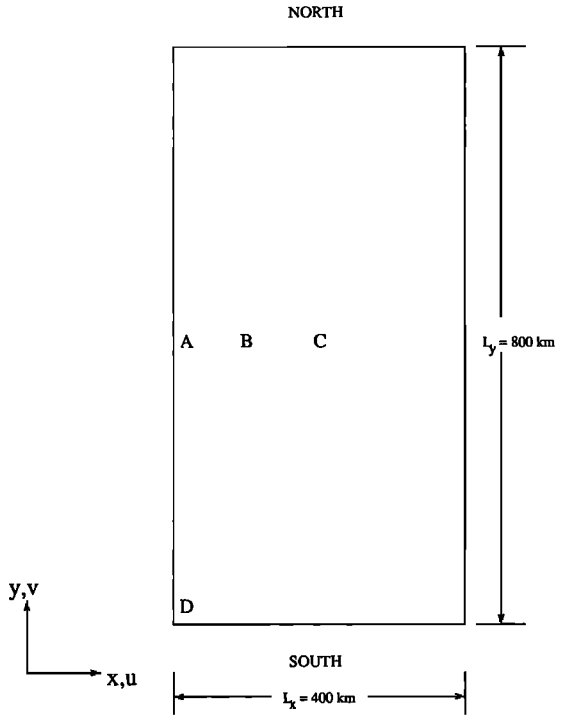

Fig. 1. Schematic of the closed rectangular basin showing the four locations at which time series of current (A, B, C) and sea level (D) are compared.

real time, and so we infer them from interior current measurements using the adjoint method of data assimilation. An efficient numerical scheme for calculating the flow field, and in particular the low-frequency, near-surface currents, is an essential element of our data assimilation scheme. For this reason, we tested Lardner's method over a range of water depths and eddy viscosities appropriate for the Scotian shelf. We found, in agreement with *Lardner* [1990, p. 22,272], that "if a smaller eddy viscosity is used, the velocity profile is more rapidly varying and more eigenfunctions are required to represent it . . . ."

The purpose of this study is to modify Lardner's method so that rapid convergence can be achieved over a wider range of water depths and eddy viscosities. We will show that this can be achieved simply by taking $\mathbf{u}_P$ to be steady Ekman flow in water of finite depth. This includes Lardner's $\mathbf{u}_P$ as a special, shallow water, case.

We note that there are similarities between our approach and that proposed recently by *Davies* [1988]. Specifically, Davies decomposes $\mathbf{u}$ into a depth-mean flow and a remainder which determines the vertical structure. This remainder, along with the bottom stress, can be calculated at each time step by numerically evaluating a set of convolution integrals [e.g., *Jelesnianski*, 1970; *Forristall*, 1974]. This bottom stress is then used in the depth-averaged model, which is run, in "leapfrog" fashion, with the model for the vertical structure. The main advantage of Davies' approach over conventional depth-averaged models is that the bottom stress is parameterized in terms of the bottom current, and this gives more realistic flow fields, particularly in shallow water. Thus Davies terms this model an "enhanced" two-dimensional model. It should be noted, however, that decomposition of the flow into a depth-mean current and a remainder does not accelerate convergence: the rate of convergence of the enhanced two-dimensional model is essentially the same as that of an equivalent three-dimensional model and hence the number of vertical structure functions required to achieve a given accuracy is the same for both.

In section 2 we briefly review the different choices of $\mathbf{u}_P$ and outline the governing equations for the remainder, $\mathbf{u}_R = \mathbf{u} - \mathbf{u}_P$. In section 3 we compare the performance of the various methods, taking as our example the case of an enclosed sea driven by a time-varying wind. Discussion of results, and suggestions for further modification of the Galerkin-spectral method, are given in section 4.

2. Basic Equations

The linearized horizontal momentum and continuity equations governing barotropic flow on the continental shelf may be written [e.g., *Davies*, 1987]

$$\frac{\partial \mathbf{u}}{\partial t} + f\mathbf{k} \times \mathbf{u} = -g\nabla\eta + \frac{1}{h^2}\frac{\partial}{\partial \sigma}\left(\mu \frac{\partial \mathbf{u}}{\partial \sigma}\right) \tag{1}$$

$$\frac{\partial \eta}{\partial t} + \nabla \cdot h \int_{-1}^{0} \mathbf{u}\, d\sigma = 0 \tag{2}$$

where $\mathbf{u} = (u, v)$ is the horizontal velocity vector, $\mathbf{k}$ is the upward unit vector, h is the water depth, η is the sea surface elevation, f is the Coriolis parameter, g is acceleration due to gravity, μ is the coefficient of vertical eddy viscosity, and ∇ is the operator $(\partial/\partial x, \partial/\partial y)$. The σ axis points upward, with $\sigma = -1$ at the seafloor and $\sigma = 0$ at the sea surface. The top and bottom boundary conditions are taken to be

$$\begin{aligned} \mu \frac{\partial \mathbf{u}}{\partial \sigma} &= h\boldsymbol{\tau} \qquad \sigma = 0 \\ \mu \frac{\partial \mathbf{u}}{\partial \sigma} &= hk\mathbf{u} \qquad \sigma = -1 \end{aligned} \tag{3}$$

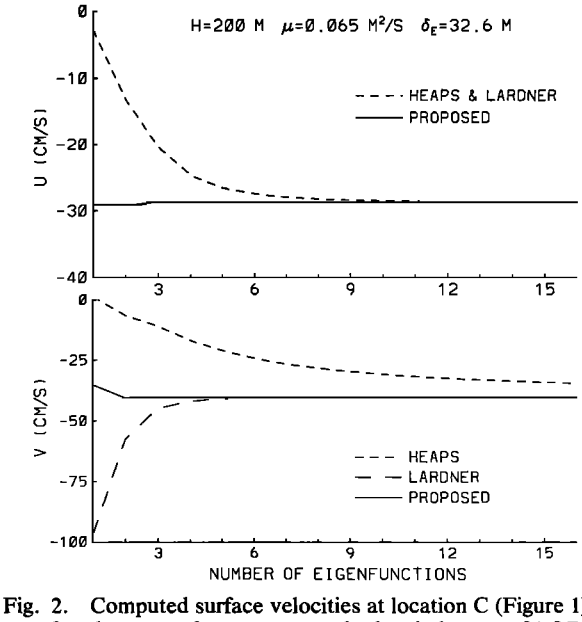

Fig. 2. Computed surface velocities at location C (Figure 1), 30 hours after the onset of a constant northerly wind stress of 1.5 Pa, as a function of the number of eigenfunctions used in the expansion. The water depth is uniform and equal to 200 m. The three lines for each panel correspond to the three methods of calculation described in the text: those of Heaps (MH) and Lardner (ML) and that proposed in this paper (MN).

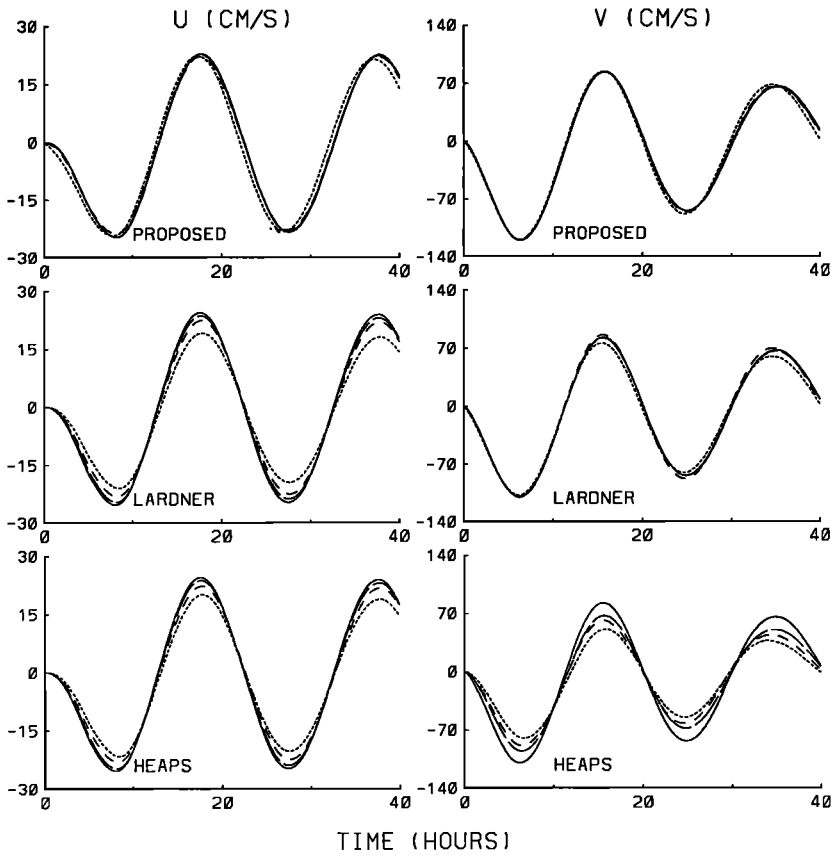

Fig. 3a

Fig. 3. Time series of surface velocity computed by the three methods using 2 (dotted curves), 3 (short-dashed curves), 4 (long-dashed curves), and 50 eigenfunctions (solid curves) at (*a*) location A, (*b*) location B, and (*c*) location C (see Figure 1). The water depth increases from 20 m at the coast to 200 m in the center of the basin according to (26). The wind forcing is zero until $t = 0$ at which it varies sinusoidally with a period of $T = 20$ hours in the y direction (see (27)). (Top) MN, (middle) ML, (bottom) MH.

where $\tau = (\tau_x, \tau_y)$ is the kinematic wind stress vector. Note that the bottom stress parameterization is linear in bottom velocity; we will discuss use of a more realistic quadratic parameterization in the final section. No-slip at the bottom boundary corresponds to the limit that k tends to infinity.

The vertical structure of **u** is often described in terms of eigenfunctions of the following Sturm-Liouville problem [e.g., *Heaps*, 1972; *Davies*, 1987]:

$$\frac{1}{h^2}\frac{\partial}{\partial\sigma}\left(\mu\frac{\partial\phi}{\partial\sigma}\right) + \lambda\phi = 0 \tag{4}$$

subject to

$$\mu\frac{\partial\phi}{\partial\sigma} = 0 \qquad \sigma = 0$$
$$\mu\frac{\partial\phi}{\partial\sigma} = hk\phi \qquad \sigma = -1 \tag{5}$$

where λ is the eigenvalue associated with the eigenfunction $\phi(\sigma)$. It should be noted that the choice of zero stress at the sea surface in (5) is the source of the poor convergence for the wind-driven problem. The main advantage of eigenfunctions is that the differential equations governing the temporal evolution of their coefficients decouple for linear models and that efficient numerical schemes have been developed to integrate them [e.g., *Heaps*, 1972; *Davies*, 1983; *Lardner*, 1990].

For constant eddy viscosity, the eigenfunctions are simply

$$\phi_r(\sigma) = \cos(\alpha_r\sigma) \qquad r = 1, 2, \cdots \tag{6}$$

where the α_r are the positive roots, in ascending order, of

$$\alpha\tan\alpha = kh/\mu \tag{7}$$

which is obtained by substituting (6) into (5). Substituting (6) into (4) gives

$$\lambda_r = \alpha_r^2\mu/h^2$$

For all r, $(r - 1)\pi < \alpha_r < (r - 1/2)\pi$ with α_r tending toward the lower limit of this range as r tends to infinity. For a no-slip bottom boundary condition, $\alpha_r = (r - 1/2)\pi$ for all r. (See *Heaps* [1972] for a full discussion of the properties of the eigenvectors and eigenvalues associated with constant μ.) For completeness, we give below the depth integrals of ϕ and ϕ^2 for constant μ, both of which will be required in our application of the Galerkin-spectral method:

$$\langle\phi_r\rangle = \sin\alpha_r/\alpha_r$$
$$\langle\phi_r^2\rangle = (2 + \sin 2\alpha_r/\alpha_r)/4 \tag{8}$$

where

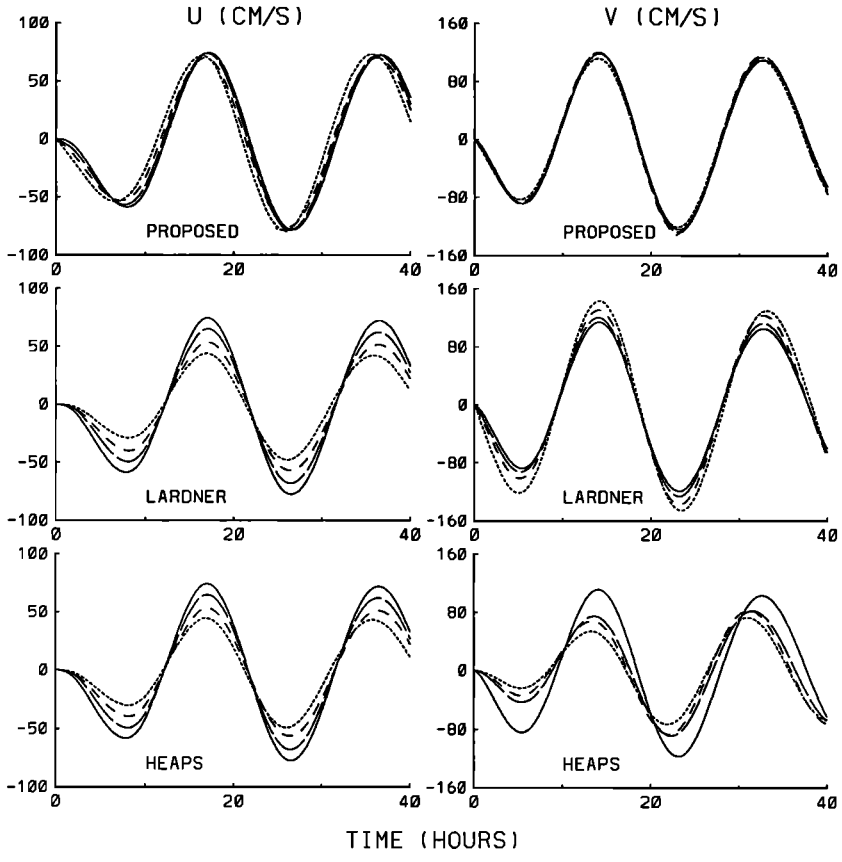

Fig. 3*b*

$$\langle\ \rangle = \int_{-1}^{0} (\ )\, d\sigma$$

Clearly, $-1 < \langle\phi_r\rangle < 1$ with the modulus of $\langle\phi_r\rangle$ eventually tending to zero with increasing r at least as quickly as r^{-1}. In contrast, $1/4 < \langle\phi_r^2\rangle < 3/4$ with $\langle\phi_r^2\rangle$ tending toward 1/2 as r tends to infinity.

2.1. *Choices of* $\mathbf{u}_P$

One problem with using cosines to describe the vertical structure of wind-driven currents is that convergence can be slow [e.g., *Davies and Owen*, 1979]. For example, *Davies* [1983] noted that, at times, even 20 cosines were insufficient to obtain an accurate representation of the surface currents. As was noted above, the problem stems from the pronounced vertical structure of the near-surface currents in deep water, coupled with the fact that the computed vertical current shear is identically zero at $\sigma = 0$ [*Heaps*, 1972; *Davies*, 1987].

Lardner's [1990] way of accelerating the convergence of the eigenfunction expansion of $\mathbf{u}$ is to first subtract a particular flow field, $\mathbf{u}_P$, to deal with the inhomogeneous surface boundary condition, and then solve for the remainder, $\mathbf{u}_R = \mathbf{u} - \mathbf{u}_P$, using the Galerkin-spectral method. Given that the components of $\mathbf{u}_R$ satisfy the same boundary conditions as ϕ, specifically (5), Lardner argued that the ϕ expansion of $\mathbf{u}_R$ should converge more rapidly than that of $\mathbf{u}$. Lardner's $\mathbf{u}_P$ is the solution of

$$\frac{1}{h^2}\frac{\partial}{\partial\sigma}\left(\mu\frac{\partial\mathbf{u}}{\partial\sigma}\right) = 0 \tag{9}$$

subject to (3). The solution, which we denote by $\mathbf{u}_P = \mathbf{u}_L$, is [*Lardner*, 1990]

$$\mathbf{u}_L = \frac{\boldsymbol{\tau}}{k} + \boldsymbol{\tau} h \int_{-1}^{\sigma} \frac{d\sigma}{\mu} \tag{10}$$

Note that $\mathbf{u}_L$ has constant horizontal shear stress through the vertical, with the surface wind stress balanced exactly by the bottom stress. Such flows are expected to occur in shallow water [e.g., *Csanady*, 1982]. However, $\mathbf{u}_L$ does not accurately describe wind-driven current profiles in deep water. To illustrate, if we assume a mid-latitude shelf of depth 200 m, a steady wind stress of 0.2 Pa, and an eddy viscosity of 0.065 m^2 s^{-1} [e.g., *Heaps*, 1972], simple Ekman theory would predict a surface current of less than 0.1 m s^{-1} at about 45° to relative to the wind, with most of the flow occurring in the top 50 m. In contrast, $\mathbf{u}_L$ gives a significantly higher, and unrealistic, surface current of 0.6 m s^{-1} in the same direction as the wind, decreasing linearly to zero at the seafloor (assuming, for simplicity, a no-slip bottom boundary condition).

An alternative $\mathbf{u}_P$, which we will show leads to more rapid convergence over a wider range of water depths and eddy viscosities, is steady Ekman flow $\mathbf{u}_E$, which is the solution of

$$\frac{1}{h^2}\frac{\partial}{\partial\sigma}\left(\mu\frac{\partial\mathbf{u}}{\partial\sigma}\right) - f\mathbf{k}\times\mathbf{u} = 0 \tag{11}$$

subject to (3). Analytical expressions for $\mathbf{u}_E$ have been obtained for various eddy viscosity profiles including a constant [e.g., *Ekman*, 1905; *Welander*, 1957], exponential [e.g., *Witten and Thomas*, 1976], and a power law [e.g., *Thomas*,

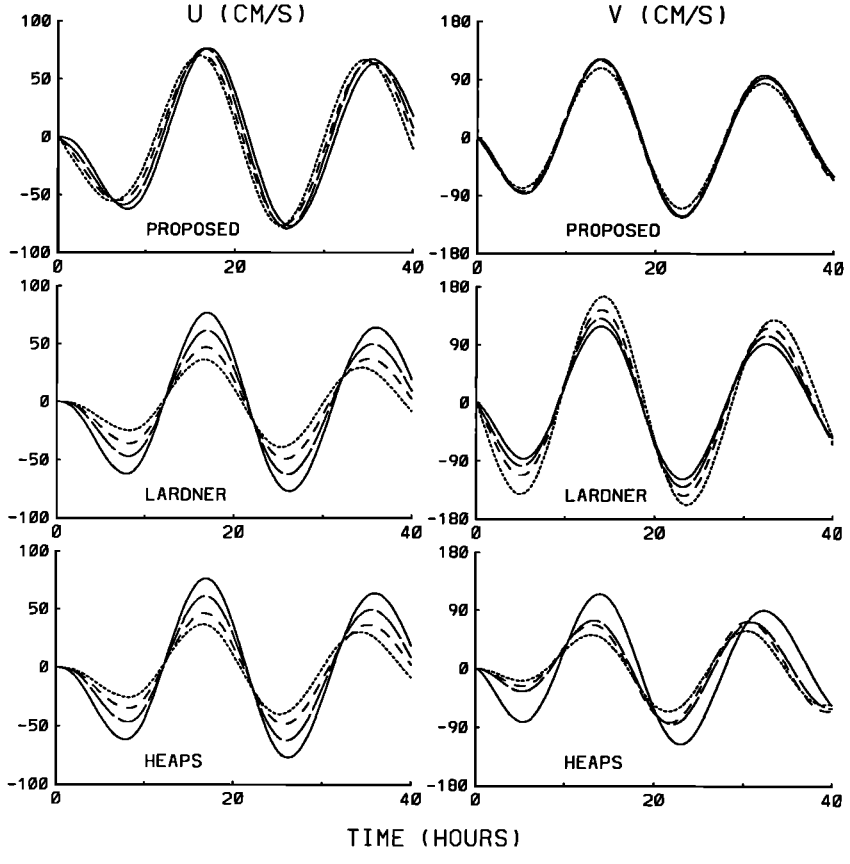

Fig. 3c

1975; *Jordan and Baker*, 1980]. For constant μ, for example, explicit expressions for u_E and v_E in terms of τ_x and τ_y can be obtained by equating the real and imaginary parts of

$$u_E + iv_E = \frac{\gamma_0}{k}\left[\frac{\cosh\ \gamma_1(1+\sigma) + \gamma_0 \sinh\ \gamma_1(1+\sigma)}{\sinh\ \gamma_1 + \gamma_0 \cosh\ \gamma_1}\right] \cdot (\tau_x + i\tau_y) \quad (12)$$

where

$$\gamma_0 = k\delta_E/\mu(1+i)$$

$$\gamma_1 = (1+i)h/\delta_E$$

and δ_E is the Ekman depth defined by

$$\delta_E = (2\mu/f)^{1/2}$$

Note that as δ_E/h tends to zero, $\mathbf{u}_E$ tends to the familiar Ekman spiral. As δ_E/h tends to infinity, $\mathbf{u}_E$ approaches $\mathbf{u}_L$. Thus the particular solution chosen by *Lardner* [1990] is the shallow water limit of (12).

In anticipation of our application of the Galerkin-spectral method in the next section we now give, for arbitrary μ, the depth averages of $\mathbf{u}_L$ and $\mathbf{u}_E$:

$$\langle \mathbf{u}_L \rangle = \frac{\boldsymbol{\tau}}{k} - \boldsymbol{\tau} h \int_{-1}^{0} \frac{\sigma}{\mu}\, d\sigma \quad (13)$$

$$\langle \mathbf{u}_E \rangle = \mathbf{k} \times [\boldsymbol{\tau}_b - \boldsymbol{\tau}]/fh \quad (14)$$

where $\boldsymbol{\tau}_b$ is the bottom stress. We will also require the following projections of $\mathbf{u}_L$ and $\mathbf{u}_E$ onto the eigenfunctions:

$$\langle \mathbf{u}_L \phi_r \rangle = \boldsymbol{\tau}/\lambda_r h \quad (15)$$

$$\langle \mathbf{u}_E \phi_r \rangle = [\lambda_r \boldsymbol{\tau} - f\mathbf{k} \times \boldsymbol{\tau}]/h(\lambda_r^2 + f^2) \quad (16)$$

2.2. *Governing Equations for* $\mathbf{u}_R$

Following *Lardner* [1990], we subtract our particular solution, $\mathbf{u}_E$, from $\mathbf{u}$ and obtain a remainder, $\mathbf{u}_R$, which satisfies the following momentum and continuity equations:

$$\frac{\partial \mathbf{u}_R}{\partial t} + f\mathbf{k} \times \mathbf{u}_R = -g\nabla\eta + \frac{1}{h^2}\frac{\partial}{\partial \sigma}\left(\mu \frac{\partial \mathbf{u}_R}{\partial \sigma}\right) - \frac{\partial \mathbf{u}_E}{\partial t} \quad (17)$$

$$\frac{\partial \eta}{\partial t} + \nabla \cdot h \int_{-1}^{0} \mathbf{u}_R\, d\sigma = -\nabla \cdot h \int_{-1}^{0} \mathbf{u}_E\, d\sigma \quad (18)$$

The top and bottom boundary conditions are

$$\mu \frac{\partial \mathbf{u}_R}{\partial \sigma} = 0 \qquad \sigma = 0$$

$$\mu \frac{\partial \mathbf{u}_R}{\partial \sigma} = hk\mathbf{u}_R \qquad \sigma = -1 \quad (19)$$

Note that by design, the boundary conditions for the components of $\mathbf{u}_R$ are identical to those of the eigenfunctions. The initial conditions corresponding to a state of rest are $\mathbf{u}_R = -\mathbf{u}_E$ at $t = 0$. Along solid lateral boundaries we will require the normal component of depth-integrated flow to vanish.

Applying the Galerkin-spectral method to the above set of equations, we first express $\mathbf{u}_R$ as a sum of eigenfunctions $\phi_s(\sigma)$ with coefficients $\mathbf{U}_s(x, y, t) = (U_s, V_s)$:

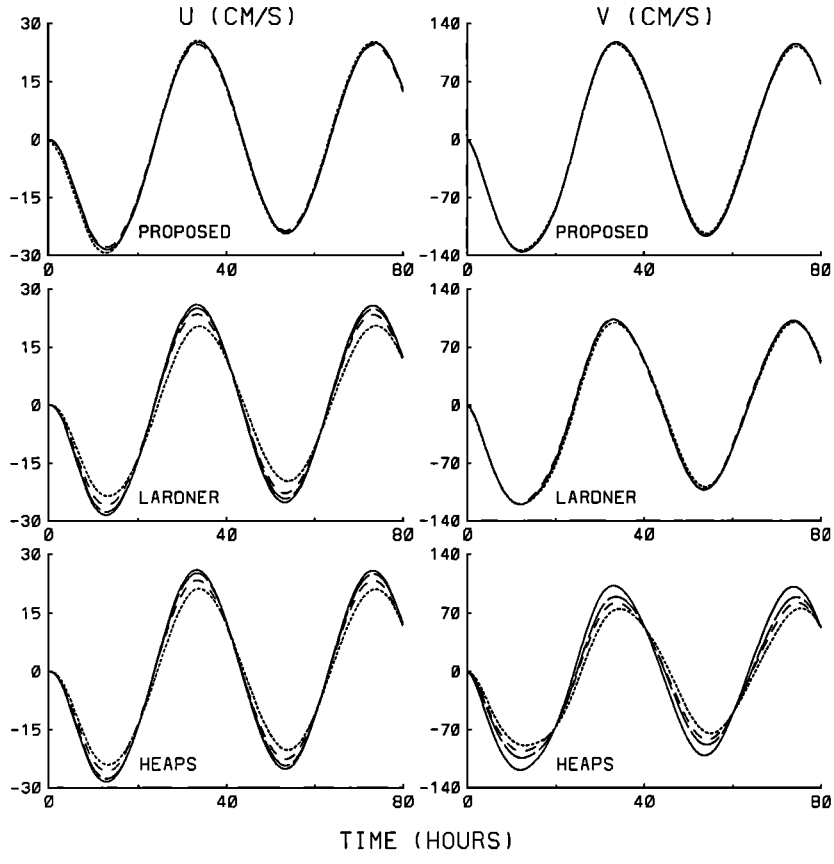

Fig. 4*a*

Fig. 4. Time series of surface velocity computed by the three methods using 2 (dotted curves), 3 (short-dashed curves), 4 (long-dashed curves), and 50 eigenfunctions (solid curves) at (*a*) location A, (*b*) location B, and (*c*) location C (see Figure 1). The water depth increases from 20 m at the coast to 200 m in the center of the basin according to (26). The wind forcing is zero until $t = 0$ at which it varies sinusoidally with a period of $T = 40$ hours in the y direction (see (27)). (Top) MN, (middle) ML, (bottom) MH.

$$\mathbf{u}_R = \sum_s \mathbf{U}_s \phi_s \tag{20}$$

We assume below that the eigenfunctions have been normalized such that $\phi(0) = 1$ and thus $\mathbf{U}_s$ may be interpreted as the contribution of the sth eigenfunction to the surface current. In the usual way, we substitute (20) into (17), multiply by $\phi_r(\sigma)$, and integrate from sea surface to seafloor to obtain the following equation governing the temporal evolution of the rth eigenfunction coefficient:

$$\frac{\partial \mathbf{U}_r}{\partial t} + f\mathbf{k} \times \mathbf{U}_r + \lambda_r \mathbf{U}_r = -g \frac{\langle \phi_r \rangle}{\langle \phi_r^2 \rangle} \nabla \eta - \frac{1}{\langle \phi_r^2 \rangle} \frac{\partial \langle \mathbf{u}_E \phi_r \rangle}{\partial t} \tag{21}$$

Note that the eigenvalue, λ_r, can be interpreted as the reciprocal of the spin-down time of $\mathbf{U}_r$. Manifestly, the forcing term is proportional to temporal changes in the projection of the Ekman solution onto the eigenfunctions, given by (16); it will, of course, vanish if the wind is steady.

The continuity equation accompanying (21) is

$$\frac{\partial \eta}{\partial t} + \sum_r \nabla \cdot h \langle \phi_r \rangle \mathbf{U}_r = -\nabla \cdot h \langle \mathbf{u}_P \rangle \tag{22}$$

with $\mathbf{u}_P = \mathbf{u}_E$ in our case. The right-hand side is proportional to the divergence of the horizontal transport carried by the Ekman flow; for $\delta_E \ll h$ it has a simple physical interpretation in terms of Ekman pumping by the top and bottom frictional boundary layers. For constant μ it is readily determined from the instantaneous wind stress by using (14) and (12).

Thus we have three ways of calculating barotropic, wind-driven currents: they differ only in the particular solution, $\mathbf{u}_P$, that is subtracted from $\mathbf{u}$ prior to the eigenfunction expansion. For convenience we list below the three equations governing the temporal evolution of $\mathbf{U}_r$, one for each method:

Heaps (MH)

$$\frac{\partial \mathbf{U}_r}{\partial t} + f\mathbf{k} \times \mathbf{U}_r + \lambda_r \mathbf{U}_r + g \frac{\langle \phi_r \rangle}{\langle \phi_r^2 \rangle} \nabla \eta = \frac{1}{\langle \phi_r^2 \rangle} \left[\frac{\boldsymbol{\tau}}{h} \right] \tag{23}$$

Lardner (ML)

$$\frac{\partial \mathbf{U}_r}{\partial t} + f\mathbf{k} \times \mathbf{U}_r + \lambda_r \mathbf{U}_r + g \frac{\langle \phi_r \rangle}{\langle \phi_r^2 \rangle} \nabla \eta = \frac{1}{\langle \phi_r^2 \rangle} \left[-\frac{\partial \langle \mathbf{u}_L \phi_r \rangle}{\partial t} - f\mathbf{k} \times \langle \mathbf{u}_L \phi_r \rangle \right] \tag{24}$$

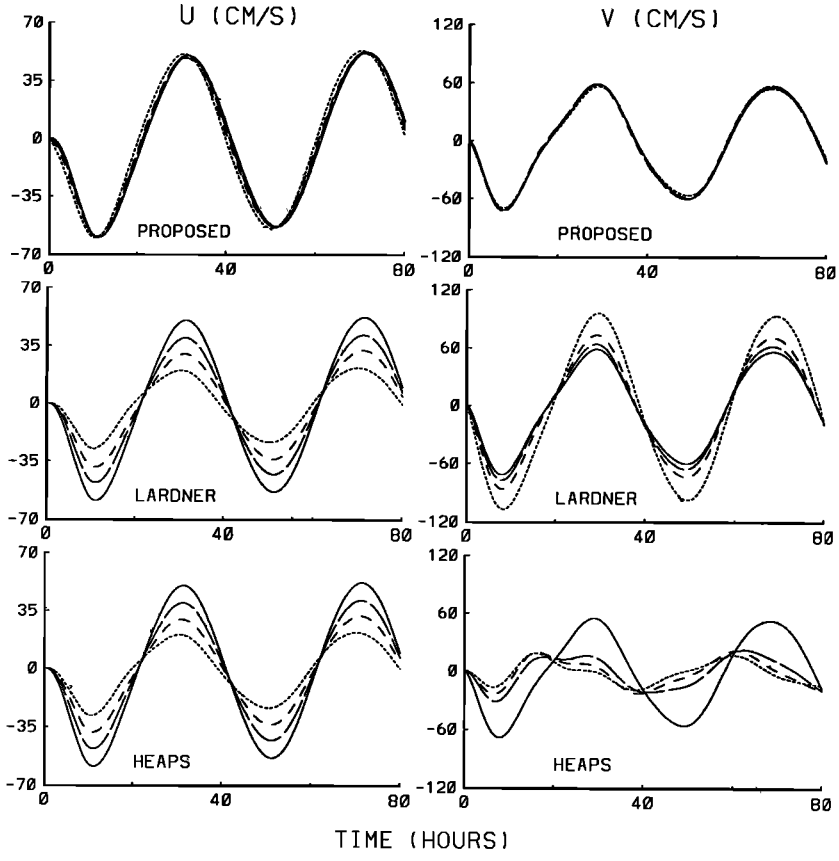

Fig. 4*b*

New (MN)

$$\frac{\partial \mathbf{U}_r}{\partial t} + f\mathbf{k} \times \mathbf{U}_r + \lambda_r \mathbf{U}_r + g \frac{\langle \phi_r \rangle}{\langle \phi_r^2 \rangle} \nabla \eta = \frac{1}{\langle \phi_r^2 \rangle} \left[- \frac{\partial \langle \mathbf{u}_E \phi_r \rangle}{\partial t} \right] \tag{25}$$

Heaps' approach requires the numerical solution of (23), and (22) with $\mathbf{u}_P = 0$, subject to appropriate initial and lateral boundary conditions. Similarly, Lardner's approach requires the numerical solution (24), and (22) with $\mathbf{u}_P = \mathbf{u}_L$. Our modification of Lardner's approach is simply to replace $\mathbf{u}_L$ with $\mathbf{u}_E$ and solve (25) and (22). For convenience we will henceforth refer to Heaps', Lardner's, and the new method as MH, ML, and MN, respectively. Note that for both ML and MN, the "forcing" depends the projections of $\mathbf{u}_P$ onto the eigenfunctions along with their depth means: explicit expressions for these quantities, in terms of τ, are given by (13)–(16).

3. Flow in a Rectangular Basin

To assess the convergence rates of the three numerical methods, we have performed a series of calculations of wind-driven flow in a rectangular basin and compared the surface velocities and elevations at four locations (Figure 1). Detailed discussions of the dynamical response of closed basins to time-dependent wind forcing have already appeared in the literature (see *Csanady* [1982] for a review); this section covers only the numerical efficiency of MH, ML, and MN.

The horizontal dimensions of the basin are 400 km in the x direction and 800 km in the y direction. These dimensions were used by *Heaps* [1972] in his pioneering study of the North Sea, and over the years they have become standard in the comparison of three-dimensional numerical models [e.g., *Davies and Owen*, 1979; *Davies*, 1983, 1988; *Lardner and Smoczynski*, 1990; *Lardner*, 1990]. We have used two types of bathymetry: a flat bottom and one that deepens toward the center. We have also used two types of wind forcing: a steady wind and a time-harmonic wind, both switched on at $t = 0$. For all model runs we assumed $f = 1.22 \times 10^{-4}$ s^{-1}, corresponding to the approximate latitude of the North Sea, $k = 0.002$ m s^{-1}, $g = 9.81$ m s^{-2}, $\rho = 1025$ kg m^{-3}, a time step of $\Delta t = 180$ s, and a horizontal grid spacing of $\Delta x = 400/9$ km and $\Delta y = 800/17$ km.

The choice of eddy viscosity can have a significant effect on the convergence rate of the ϕ_r expansion of $\mathbf{u}$ [e.g., *Davies*, 1987; *Lardner*, 1990]. A wide range of values have been used in the past. *Heaps* [1972], for example, used eddy viscosities which were constant in the vertical, ranging in value from 0.03 to 0.26 m^2 s^{-1}. Two constant values of μ have been used in this study: the highest value of $\mu = 0.065$ m^2 s^{-1} was used for the uniform water depth calculation and a lower value of $\mu = 0.0244$ m^2 s^{-1} was used for the variable bathymetry calculation. The main reason for choosing a lower value of μ in the second case is to give a minimum value for h/δ_E of approximately 1. Note that for constant μ, eigenfunctions and eigenvalues depend on the parameter kh/μ. Some modelers have assumed this parameter to be independent of (x, y, t) and gone on to develop highly efficient numerical schemes [e.g., *Heaps*, 1972; *Davies and Furnes*, 1980; *Hukuda et al.*, 1989; *Lardner*, 1990]. Although this may be reasonable for small variations of h, it would

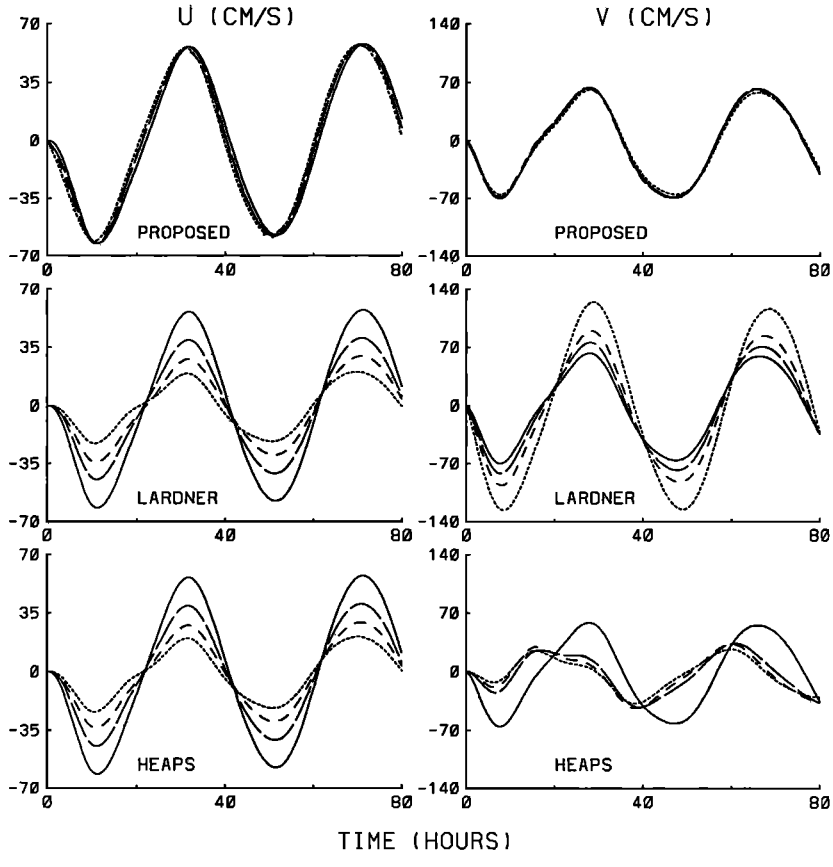

Fig. 4c

appear unrealistic to assume that μ is proportional to kh over water depths ranging from 20 to 200 m, typical of continental shelf seas. Thus we have allowed kh/μ to vary with x and y and calculated the ϕ_r and α_r for each grid point, prior to the time integration of the momentum and continuity equations.

All three numerical schemes are based on an Arakawa C grid with U_r, V_r and η specified at different points. Forward time stepping is used for the time derivative terms, and centered time stepping is used for the friction terms (to avoid computational instabilities [*Heaps*, 1972]). The Coriolis terms are treated in the manner proposed by *Heaps* [1972]. Specifically, the values of fU_r and fV_r are averaged over four neighboring grid points. (Note, however, that the Coriolis terms for the steady Ekman flow are calculated on the u, v grid without averaging: the impact of this slight difference on the calculated flow fields was found to be insignificant.) To optimize the model we have also followed *Lardner* [1990] by updating V_r on the odd time steps using the most recent values of fU_r and updating U_r on the even time steps using the most recent values of fV_r. We also note here that *Heaps* [1972] introduced a correction term for the truncation error in the expansion of the flow in the wind direction. This correction has not been included in any of the three methods.

3.1. *Flat Bottom and Steady Wind*

We assume $h = 200$ m everywhere. In accord with previous model comparisons based on the North Sea rectangle, we assume that $\mu = 0.065$ m^2 s^{-1}, suddenly impose a northerly wind stress of 1.5 Pa and compare the response of current and sea level at $t = 30$ hours. Note that for this example $\delta_E/h = 0.16$.

Surface velocities in the center of the basin, as a function of the number of eigenfunctions (m), are shown in Figure 2. The surface velocity computed by MN converges rapidly: two or three eigenfunctions would appear to be sufficient. In contrast, ML requires at least seven eigenfunctions to be within 0.01 cm s^{-1} of the true solution, while MH needs even more eigenfunctions ($m > 15$), particularly for that flow component in the same direction as the wind. In an additional series of calculations, we also found that the number of eigenfunctions required to achieve a given accuracy increased with h/δ_E for both MH and ML; in contrast, the number of eigenfunctions required by MN was relatively insensitive to this ratio. We also found that ML and MN both worked well if h/δ_E was close to, or less than, unity. For example, with $h/\delta_E = 1.7$, only three eigenfunctions were needed by these two methods to achieve an accuracy better than 0.01 cm s^{-1}, while 25 were needed by MH.

It is clear that the situation described above is highly idealized, in terms of both the wind forcing and the bathymetry. It is also biased in favor of MN because the circulation in the middle of the basin after 30 hours is close to steady Ekman flow, the particular solution used in MN. We have therefore compared the performance of the three methods using more a realistic bottom topography, giving a range of δ_E/h, and a time-varying wind.

3.2. *Variable Bathymetry and Time-Harmonic Wind*

We assume that the water depth (in meters) increases from 20 along the lateral boundaries to 200 in the center of the basin according to

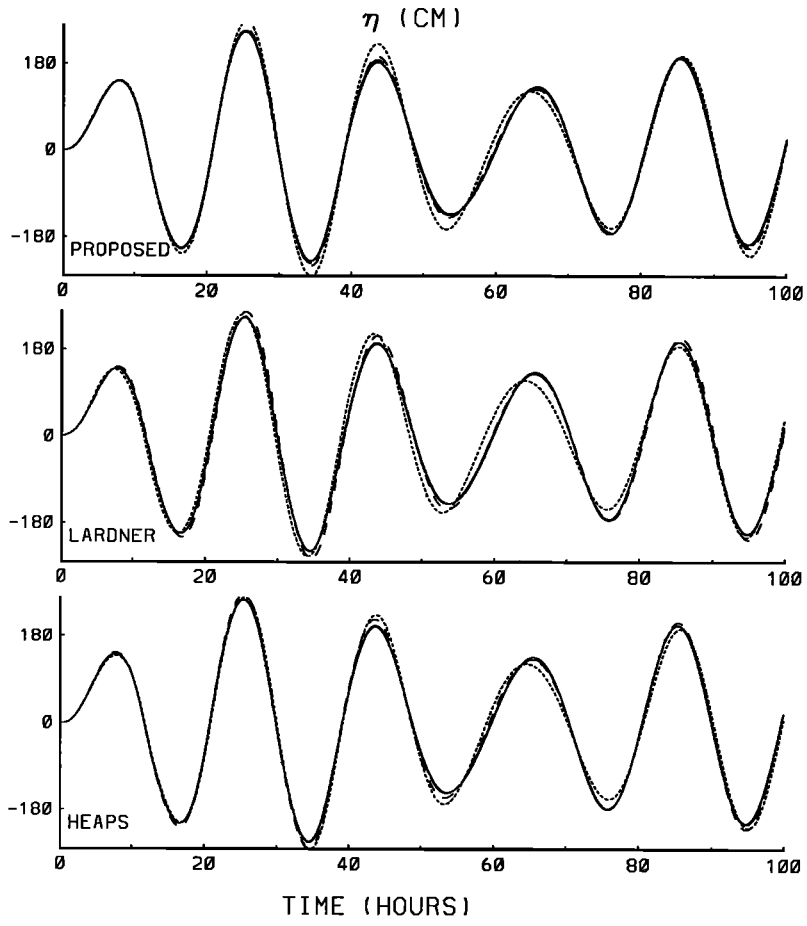

Fig. 5. Time series of surface elevation computed using the three methods at location D with $T = 20$ hours. Otherwise as in Figure 3.

$$h(x, y) = 20 + 180 \sin\left(\pi \frac{x}{L_x}\right) \sin\left(\pi \frac{y}{L_y}\right) \quad (26)$$

We also assume that the eddy viscosity is constant and equal to 0.0244 $m^2\ s^{-1}$. Note that kh/μ is no longer constant and so both the eigenvalues (λ_r) and eigenfunctions (ϕ_r) vary across the model domain. They were calculated and stored prior to the integration of the momentum and continuity equations. The east-west wind stress is again assumed equal to zero and the north-south wind stress (in pascals) is defined by

$$\rho\tau_y = -1.5 \sin\left(\frac{2\pi t}{T}\right) \qquad t > 0 \quad (27)$$

where T is the wind period. The initial conditions were taken to be a state of rest.

Surface currents at three different locations (shallow, intermediate and deep; see Figure 1) are shown in Figure 3 for forcing by a subinertial wind with $T = 20$ hours. The different line types corresponds to different numbers of eigenfunctions used in the expansion of $\mathbf{u}_R$: $m = 2$, 3, 4, and 50.

At the shallow location A ($h = 50$ m, $h/\delta_E \approx 2.5$) both ML and MN perform well: four eigenfunctions would appear to be sufficient in the sense that the curves for $m = 4$ and $m = 50$ are almost identical. In contrast, MH seriously underestimates the surface current in the direction of the wind with $m = 4$. Note that the u component according to ML and MH are identical. The reason is that $\mathbf{u}_L$ is zero perpendicular to wind, and hence the governing equation for u_R is the same for both ML and MH. We will return to this point in the next section.

At the intermediate depth location B ($h = 160$ m, $h/\delta_E \approx 8$) and the deep location C ($h = 200$ m, $h/\delta_E \approx 10$) we find that MN performs well, even though the wind is now unsteady; again $m = 4$ would appear to be sufficient. ML is less successful at these locations, particularly for that component of flow perpendicular to the wind: at C, for example, the first peak in u is underestimated by 53% with $m = 2$ and by 20% with $m = 4$. It is also clear that the v-component from MH converges slowly compared to both ML and MN.

Surface currents driven by a lower frequency wind ($T = 40$ hours) are shown in Figure 4. Overall, MN performs marginally better for $T = 40$ compared with $T = 20$ hours. This is to be expected, given that the forcing terms in the momentum equations are proportional to the rate of change of wind stress. In contrast, MH and ML are less successful with increasing T, particularly in deeper water. For example, at C, ML underestimates the first peak in u by 66% with $m = 2$, and about 30% with $m = 4$. It is also clear that MH not only underestimates the speed but also fails to capture the shape of the v time series with $m = 4$. In fact, there are still slight differences between the v calculated with MH and the other two methods, even with m as high as 50.

Plots of surface elevations at location D for $T = 20$ and $T = 40$ hours are shown in Figures 5 and 6. All three

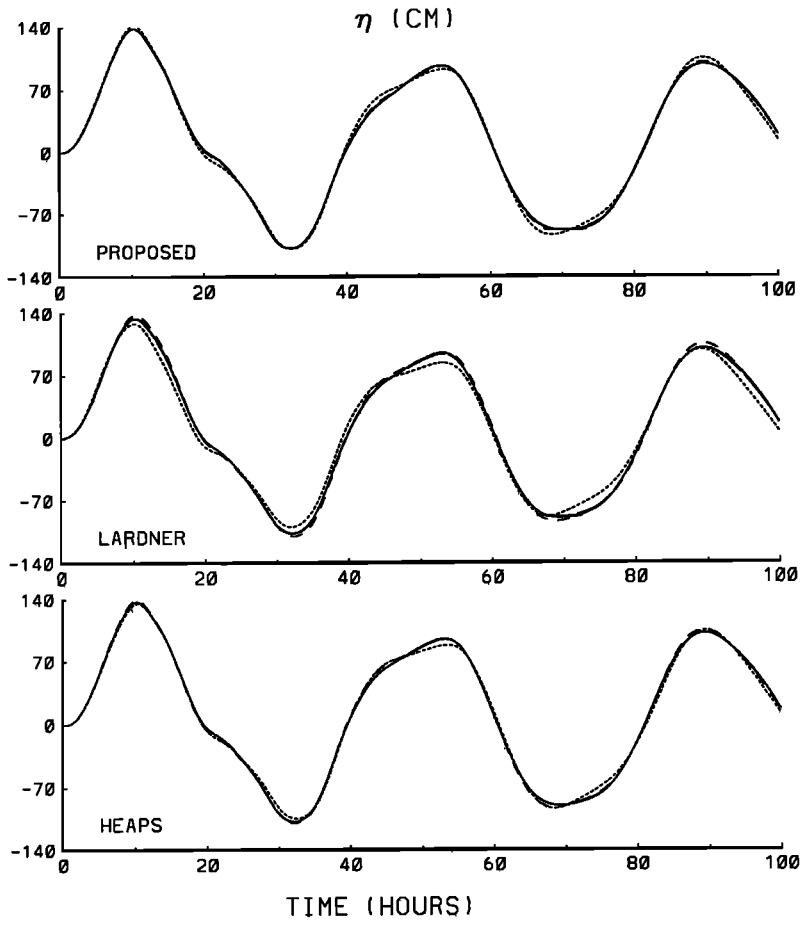

Fig. 6. Time series of surface elevation computed using the three methods at location D with $T = 40$ hours. Otherwise as in Figure 4.

methods perform well, for reasons discussed in the next section.

4. Summary and Discussion

We have compared the convergence rate of the expansion

$$\mathbf{u} = \mathbf{u}_P + \sum_s \mathbf{U}_s \phi_s(\sigma) \tag{28}$$

for three choices of $\mathbf{u}_P$, taking as our example wind-driven flow in a rectangular basin. The special case of $\mathbf{u}_P = 0$ corresponds to the "traditional" method (MH) introduced by *Heaps* [1972]. Lardner's method (ML) takes $\mathbf{u}_P = \mathbf{u}_L$, where $\mathbf{u}_L$ has constant horizontal shear stress through the vertical. Our modification (MN) of Lardner's method is to take $\mathbf{u}_P = \mathbf{u}_E$, where $\mathbf{u}_E$ is steady Ekman flow in water of finite depth. MH has the slowest convergence rate of all three methods, particularly for that component of flow in the same direction as the wind. ML is highly effective at accelerating convergence in shallow water, but is less effective in deep water. The convergence rate in the direction perpendicular to the wind is the same for both MH and ML. MN increases the rate of convergence in both shallow and deep water, and for flow both parallel and perpendicular to the wind. Thus our overall conclusion, based on the numerical simulations given above, is that removal of steady Ekman flow prior to the application of the Galerkin-spectral method is a straightforward and effective way of reducing the number of vertical structure functions required to describe the wind-driven component of the flow. We are presently using this approach to hindcast the time-varying, three-dimensional circulation on the Scotian shelf using observed winds and are finding that accurate results can be obtained with as few as four eigenfunctions.

To understand and generalize the results of the numerical simulations it is useful to consider the special case of steady, wind-driven flow. To keep the discussion as simple as possible, we will assume a no-slip bottom boundary condition and take μ to be constant. It is straightforward to show that under these conditions, the eigenfunction coefficients for MH are

$$\mathbf{U}_r = -\frac{2\langle\phi_r\rangle}{(1+\delta_r^4)}\left[\delta_r^2 \frac{g}{f}\nabla\eta - \mathbf{k}\times\frac{g}{f}\nabla\eta\right] + \frac{2}{(1+\delta_r^4)}\left[\delta_r^2\frac{\tau}{fh} - \mathbf{k}\times\frac{\tau}{fh}\right] \tag{29}$$

where

$$\delta_r = (r - 1/2)\frac{\pi}{2^{1/2}}\frac{\delta_E}{h}$$

Thus given $\nabla\eta$ and τ, it is straightforward to calculate all the $\mathbf{U}_r$ and thus reconstruct the full velocity profile. The sea level gradient can be obtained by substituting (29) into the continuity equation (22), with $\mathbf{u}_P = 0$, and solving the

resulting elliptic equation for η. Thus for the present discussion of convergence rates, we can think of $\nabla\eta$ as a forcing term, similar to τ. However, given that $\nabla\eta$, and hence its contribution to $\mathbf{U}_r$, is the same for all three methods, the following discussion will focus primarily on the wind-driven component of $\mathbf{U}_r$ because this will determine the differences in convergence rate.

As r tends to infinity, δ_r increases as r. Thus it is clear from (29) that the wind-driven component of $\mathbf{U}_r$ in the wind direction will eventually decrease as r^{-2} and the component perpendicular to the wind will decrease as r^{-4}. This explains why the surface currents calculated by MH converge relatively slowly in the wind direction. Consider now the effect of decreasing δ_E/h. Given that $|\tau|/f\delta_E$ is the natural scale for surface wind-driven currents in deep water, it is clear from (29) that the component of $\mathbf{U}_r$ in the wind direction varies relative to this scale as δ_E^{-1}. Thus we should expect, and indeed have found in our simulations, that the surface currents calculated by MH will converge more slowly in deeper water.

There are several ways of dealing with the slow convergence of the wind-driven component of the flow. The most direct way is to include more eigenfunctions although this will obviously increase the computational burden. Alternatively, the ϕ_r can be replaced by functions better equipped to describe the high shear associated with near-surface, wind-driven currents. For example, *Davies and Owen* [1979] have shown that Chebyshev and Legendre polynomials form a particularly effective basis sets. The approach proposed recently by *Lardner* [1990], and the subject of this study, involves the subtraction of a particular solution from $\mathbf{u}$ prior to its eigenfunction expansion. For steady flow, the eigenfunction coefficients for ML are

$$\mathbf{U}_r = -\frac{2\langle\phi_r\rangle}{(1+\delta_r^4)}\left[\delta_r^2\frac{g}{f}\nabla\eta - \mathbf{k}\times\frac{g}{f}\nabla\eta\right] + \frac{2}{(1+\delta_r^4)}\left[-\delta_r^{-2}\frac{\tau}{fh} - \mathbf{k}\times\frac{\tau}{fh}\right] \quad (30)$$

The only difference with MH is the coefficient multiplying the τ term: it has changed from δ_r^2 to $-\delta_r^{-2}$. Given that δ_r is proportional to r, it follows that convergence for the wind-driven component of the flow in the wind direction has been accelerated. In fact, the contribution of the rth eigenfunction to the surface current in the wind direction decreases as r^{-6} with increasing r, compared to r^{-2} for MH. However, note that the convergence rate for the flow perpendicular to the wind is the same for both MH and ML. Both of these features were evident in our numerical simulations.

The convergence rate for MH and ML is slowest in deep water i.e., for small δ_E/h. Physically, the problem stems from the inability of the low-order cosines to capture the highly structured surface Ekman layer in deep water. Our solution to this problem has been to replace Lardner's particular solution with steady Ekman flow in water of finite depth. The rationale is simple: subtraction of steady Ekman flow, in addition to dealing with the surface boundary condition, removes much of the vertical structure in the wind-driven surface flow, leaving a relatively smooth "remainder" which can be well described by relatively few eigenfunctions. For steady flow, the eigenfunction coefficients for MN are

$$\mathbf{U}_r = -\frac{2\langle\phi_r\rangle}{(1+\delta_r^4)}\left[\delta_r^2\frac{g}{f}\nabla\eta - \mathbf{k}\times\frac{g}{f}\nabla\eta\right] \quad (31)$$

Note that $\mathbf{U}_r$ is determined solely by η which, in turn, is forced by the initial and lateral boundary conditions and the transport divergence term in the continuity equation. Given η and its gradient are identical for all three approaches, MH must have the most rapid convergence, at least for steady flow. From the continuity equation, it is also clear that changes in η are determined by transport divergences and thus will be dominated by contributions from the low-order eigenfunctions. This is confirmed by the close agreement between the sea levels calculated using 4 and 50 eigenfunctions.

We assumed that the eigenfunctions satisfy the slip bottom boundary condition exactly. The advantage of this assumption is that the equations governing the temporal evolution of $\mathbf{U}_r$ decouple and can be solved efficiently. There are, however, several disadvantages. First, the eigenfunctions and the eigenvalues will, in general, depend on the eddy viscosity profile and water depth. This means that they have to be calculated separately for each grid point. Second, the bottom stress parameterization is necessarily linear in bottom velocity, and yet it can be argued that a quadratic formulation is more appropriate. Third, the time-splitting technique can not be used, since the term involving the pressure gradient appears in the governing equations for the coefficients of high modes. *Davies* [1988] shows how these disadvantages can be overcome for the traditional method, MH, by (1) requiring that the eigenfunctions satisfy a zero-stress bottom boundary and (2) including the bottom stress explicitly in the $\mathbf{U}_r$ equations. This ensures that the eigenfunctions depend only on the shape of the eddy viscosity profile and the pressure gradient does not affect the coefficients of the second and higher modes. This leads to Davies' enhanced two-dimensional model discussed in the introduction. We conclude by noting that both ML and MN can be modified in a similar fashion, and thus extended to accommodate arbitrary bottom stress formulations and time splitting, while retaining the advantage of faster convergence for the wind-driven component of the flow.

Acknowledgments. The authors are grateful to two anonymous reviewers, Alan Davies, and Richard Greatbatch for their very helpful comments on the manuscript. This work has been funded by OPEN, one of the 15 networks of centers of excellence supported by the Government of Canada.

REFERENCES

Csanady, G. T., *Circulation in the Coastal Ocean*, 279 pp., D. Reidel, Norwell, Mass., 1982.

Davies, A. M., On formulating a three-dimensional hydrodynamic sea model with an arbitrary variation of eddy viscosity, *Comp. Methods Appl. Mech. Eng.*, *22*, 187–211, 1980.

Davies, A. M., Formulation of a linear three-dimensional hydrodynamic sea model using a Galerkin-eigenfunction method, *Int. J. Numer. Methods Fluids*, *3*, 33–60, 1983.

Davies, A. M., Spectral models in continental shelf sea oceanography, in *Three-Dimensional Coastal Ocean Models, Coastal Estuarine Sci.*, vol. 4, edited by N. S. Heaps, pp. 71–106, AGU, Washington, D. C., 1987.

Davies, A. M., On formulating two-dimensional vertically integrated hydrodynamic numerical models with an enhanced representation of bed stress, *J. Geophys. Res.*, *93*, 1241–1263, 1988.

Davies, A. M., Solution of the 3D linear hydrodynamic equations

using an enhanced eigenfunction approach, *Int. J. Numer. Methods Fluids*, *13*, 235–250, 1991.
Davies, A. M., Modelling currents in highly sheared surface and bed boundary layers, *Cont. Shelf Res.*, *12*, 189–211, 1992.
Davies, A. M., and G. K. Furnes, Observed and computed M_2 tidal currents in the North Sea, *J. Phys. Oceanogr.*, *10*, 237–257, 1980.
Davies, A. M., and A. Owen, Three dimensional numerical sea model using the Galerkin method with a polynomial basis set, *Appl. Math. Modell.*, *3*, 421–428, 1979.
Davies, A. M., and C. V. Stephens, Comparison of the finite difference and Galerkin methods as applied to the solution of the hydrodynamic equations, *Appl. Math. Modell.*, *7*, 226–240, 1983.
Ekman, V. W., On the influence of the Earth's rotation on ocean currents, *Arch. Math. Astron. Fys.*, *2*, 1–53, 1905.
Forristall, G. Z., Three-dimensional structure of storm-generated currents, *J. Geophys. Res.*, *79*, 2721–2729, 1974.
Furnes, G., A three-dimensional numerical sea model with eddy viscosity varying piecewise linearly in the vertical, *Cont. Shelf Res.*, *2*, 231–241, 1983.
Heaps, N. S., On the numerical solution of the three-dimensional hydrodynamical equations for tides and storm surges, *Mem. Soc. R. Sci. Liege*, *Ser. 6*, 2, 143–180, 1972.
Hukuda, H., R. J. Greatbatch, and A. E. Hay, A simple three-dimensional model of the circulation off Newfoundland, *J. Geophys. Res.*, *94*, 12,607–12,618, 1989.
Jelesnianski, C. P., Bottom stress time history in linearized equations of motion for storm surges, *Mon. Weather Rev.*, *98*, 462–478, 1970.
Jordan, T. F., and J. R. Baker, Vertical structure of time-dependent flow dominated by friction in a well-mixed fluid, *J. Phys. Oceanogr.*, *10*, 1091–1103, 1980.
Lardner, R. W., Numerical solution of the linearized three-dimensional tidal equations using eddy viscosity eigenfunctions, *J. Geophys. Res.*, *95*, 22,269–22,274, 1990.
Lardner, R. W., and P. Smoczynski, A vertical/horizontal splitting algorithm for three-dimensional tidal and storm surge computations, *Proc. R. Soc. London*, *Ser. A*, 430, 263–283, 1990.
Thomas, J. H., A theory of steady wind-driven currents in shallow water with variable eddy viscosity, *J. Phys. Oceanogr.*, *5*, 136–142, 1975.
Welander, P., Wind action on a shallow sea: Some generalizations of Ekman's theory, *Tellus*, *9*, 45–52, 1957.
Witten, A. J., and J. H. Thomas, Steady wind-driven currents in a large lake with depth-dependent eddy viscosity, *J. Phys. Oceanogr.*, *6*, 85–92, 1976.
Zitman, T. J., Quasi three-dimensional current modelling based on a modified version of Davies' shapefunction approach, *Cont. Shelf Res.*, *12*, 143–158, 1992.

J. Sheng and K. R. Thompson, Department of Oceanography, Dalhousie University, Halifax, Nova Scotia, Canada B3H 4J1.

(Received July 1, 1992;
revised December 3, 1992;
accepted December 4, 1992.)